

# Failure Analysis of GaN-Based Current-Injected Vertical-Cavity Surface-Emitting Lasers

Joachim Piprek \*

Materials Department, University of California, Santa Barbara, CA 93106

## ABSTRACT

This paper investigates internal physical mechanisms that have thus far prevented current-injected InGaN/GaN vertical-cavity surface-emitting lasers (VCSELs) from lasing. Advanced device simulation is applied to a realistic VCSEL design. Several obstacles to lasing are identified, including current leakage, lateral carrier non-uniformity, and self-heating during pulsed operation.

**Keywords:** GaN-based light emitter, vertical-cavity surface-emitting laser, VCSEL, InGaN quantum wells, current leakage, carrier non-uniformity, self-heating, numerical simulation

## 1. INTRODUCTION

Vertical-cavity surface-emitting lasers (VCSELs) are expected to exhibit several advantages over their edge-emitting counterparts, including lower manufacturing costs, circular output beams, and longer lifetime. In contrast to the great success of GaAs-based VCSELs in recent years, GaN-based VCSELs face significant challenges and only optically pumped devices have been reported thus far.<sup>1</sup> Discussed reasons for the failure of current-injected GaN-VCSELs include the high threshold carrier density which is typical for all GaN-based lasers, the high optical loss due to insufficient reflectance of native AlGaN/GaN distributed Bragg reflectors (DBRs), the low conductivity of p-GaN, and the resistance of GaN to conventional wet etching. Using advanced numerical simulation, we investigate the internal device physics of a realistic GaN-VCSEL to identify and analyze physical mechanisms that prevent such devices from lasing. The device structure is described in Section 2, followed by an outline of the theoretical model and a discussion of material parameters in Section 3. The simulation results are analyzed in Section 4.

## 2. DEVICE STRUCTURE

As practical device example, we use an injection-type GaN-VCSEL which was previously designed, fabricated, and characterized.<sup>2</sup> Figure 1 shows the schematic design of this device as grown by MOCVD on sapphire. The multi-quantum well (MQW) active region consists of five 4-nm-thick  $In_{0.1}Ga_{0.9}N$  quantum wells and 8-nm-wide  $In_{0.035}Ga_{0.965}N$  barriers and it is covered by a 20-nm p-doped  $Al_{0.18}Ga_{0.82}N$  electron stopper layer to reduce electron leakage into the p-GaN spacer layer. Indium tin oxide (ITO) is employed to confine the current injection to an aperture of 2  $\mu m$  to 10  $\mu m$  diameter. The top metal ring contact confines the optical mode diameter to about 12  $\mu m$ . Eleven-period dielectric DBRs are used on both sides which exhibit a high reflectance above 99%. Due to common difficulties with thinning GaN in a well-controlled fashion, the cavity length is as large as 5.5  $\mu m$ . The measured longitudinal mode spacing is correspondingly small (4-5 nm) which eliminates the usual VCSEL design challenge of aligning gain peak and cavity mode. The dense mode spectrum also reduces the temperature sensitivity of this VCSEL.<sup>3</sup>

---

\* E-mail: piprek@ieee.org

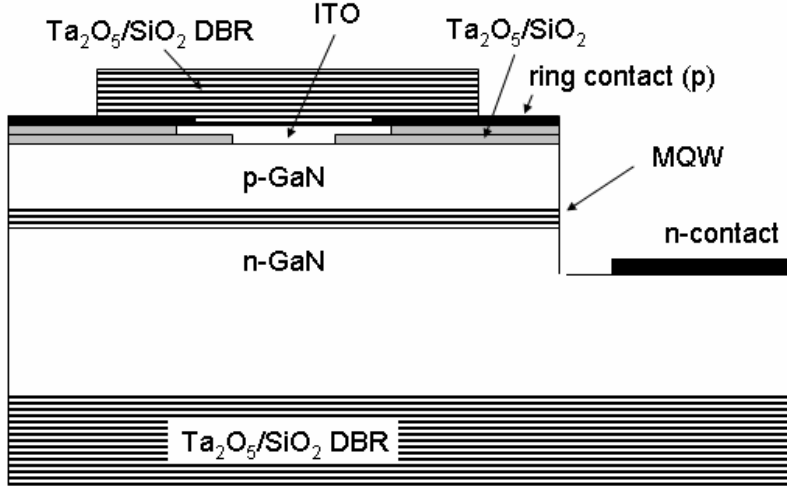


Fig. 1: Schematic VCSEL design.<sup>2</sup>

Parameter	d	N	$\mu$	n	k
Unit	$\mu\text{m}$	$\text{cm}^{-3}$	$\text{cm}^2/\text{Vs}$		$\text{W}/\text{cm K}$
$\text{SiO}_2$	0.070	-	-	1.47	0.01
$\text{Ta}_2\text{O}_5$	0.047	-	-	2.2	0.01
n-ITO (contact)	0.04	$1.0 \cdot 10^{19}$	1000	2.1	0.01
p-GaN (spacer)	0.54	$4.0 \cdot 10^{17}$	10	2.55	1.3
p-Al <sub>0.18</sub> Ga <sub>0.82</sub> N (stopper)	0.02	$1.0 \cdot 10^{16}$	5	2.27	0.8
n-In <sub>0.035</sub> Ga <sub>0.965</sub> N (barrier)	0.008	$1.0 \cdot 10^{18}$	400	2.8	0.2
In <sub>0.1</sub> Ga <sub>0.9</sub> N (quantum well)	0.004	-	p:2	2.8	0.2
n-In <sub>0.035</sub> Ga <sub>0.965</sub> N (barrier)	0.008	$1.0 \cdot 10^{18}$	400	2.8	0.2
n-GaN (spacer, contact)	5.3	$2.5 \cdot 10^{18}$	400	2.55	1.3
$\text{SiO}_2$	0.070	-	-	1.47	0.01
$\text{Ta}_2\text{O}_5$	0.047	-	-	2.2	0.01

Tab. 1: VCSEL layer structure <sup>2</sup> and parameters as used in the simulation (d - thickness; N – carrier concentration from doping;  $\mu$  - carrier mobility, n – refractive index at 400 nm wavelength; k – thermal conductivity).

### 3. THEORETICAL MODEL AND MATERIAL PARAMETERS

We here employ different physics-based software packages which we tailor to the specific needs of this investigation. As the VCSEL exhibits cylinder symmetry, two-dimensional (2D) device simulation with the vertical coordinate z and the lateral radius r is chosen. PICS3D <sup>4</sup> self-consistently combines the computation of semiconductor transport equations, quantum well bandstructure, optical gain, and optical mode. The transport model includes drift and diffusion of electrons and holes, Fermi statistics, built-in polarization and thermionic emission at hetero-interfaces, as well as spontaneous and defect-related Shockley-Read-Hall (SRH) recombination of carriers. For the quantum wells, Schrödinger and Poisson equations are solved iteratively to account for the quantum well deformation with changing device bias. Stimulated emission of photons within the quantum well is calculated by a free carrier model including the wurtzite energy band structure. A very similar model was previously used to study InGaN/GaN in-plane lasers, resulting in excellent agreement between measurements and simulations.<sup>5</sup> However, we here perform the thermal simulation separately using the multi-physics simulation software FEMLAB.<sup>6</sup>

An important issue in any device simulation is the selection of appropriate values for the various material parameters employed in the simulation. Published values for many parameters of GaN-based compounds vary substantially in the literature. We mainly employ the nitride parameters given in Refs.<sup>5,7</sup> some of which are listed in Table 1. However, the crucial issue of strong self-polarization observed in nitride compounds should be addressed in more detail.

Built-in interface charges due to spontaneous and piezoelectric polarization are known to influence the performance of nitride devices.<sup>8</sup> Much theoretical and experimental research has been committed to the unusual built-in polarization strength in GaN-based alloys. Figure 2 shows the theoretically predicted interface charge density and the corresponding built-in field as function of alloy composition.<sup>9</sup> Table 2 lists the fixed charges calculated for our interfaces, which result in a built-in quantum well field of 1.8 MV/cm. This strong field leads to a separation of electrons and holes within the quantum well and thereby to a reduction of the photon emission rate. However, experimental investigations of similar quantum wells often give weaker built-in fields than predicted, ranging from 20%<sup>10</sup> to 80%<sup>11</sup> of the theoretical value, with typical results near 50%.<sup>12</sup> This broad variation has been attributed to partial compensation of the polarization field by fixed defect and interface charges<sup>13</sup> or to inappropriate analysis of measured data.<sup>14</sup> On the other hand, the theoretical polarization formulas may deviate from reality, especially for InGaN, as only AlGaN measurements have been used for validation.<sup>9</sup> Since the actual magnitude of built-in polarization in our device is unknown, we are using the polarization charges as a parameter in some of our simulations.

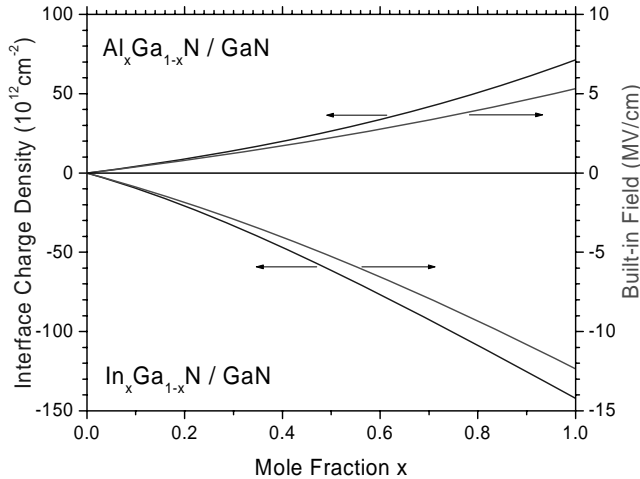


Fig. 2: Polarization charges and corresponding built-in field at InGaN/GaN and AlGaN/GaN interfaces.<sup>9</sup>

Interface	Polarization Charge
GaN/In <sub>0.035</sub> Ga <sub>0.965</sub> N	- 3.2 x 10 <sup>12</sup> cm <sup>-2</sup>
In <sub>0.035</sub> Ga <sub>0.965</sub> N/In <sub>0.1</sub> Ga <sub>0.9</sub> N	- 6.5 x 10 <sup>12</sup> cm <sup>-2</sup>
In <sub>0.1</sub> Ga <sub>0.9</sub> N/In <sub>0.035</sub> Ga <sub>0.965</sub> N	+ 6.5 x 10 <sup>12</sup> cm <sup>-2</sup>
In <sub>0.35</sub> Ga <sub>0.965</sub> N/Al <sub>0.18</sub> Ga <sub>0.82</sub> N	+ 11 x 10 <sup>12</sup> cm <sup>-2</sup>
Al <sub>0.18</sub> Ga <sub>0.82</sub> N/ GaN	- 7.8 x 10 <sup>12</sup> cm <sup>-2</sup>

Table 2: Fixed polarization charges as calculated for the semiconductor interfaces in our VCSEL.

## 4. SIMULATION RESULTS AND ANALYSIS

### 4.1 Current Confinement Effects

The optical mode size in our device is laterally confined by the top ring contact with about 12  $\mu\text{m}$  aperture (cf. Fig. 1). Hole injection is provided by the top ITO layer with an aperture between 2  $\mu\text{m}$  and 10  $\mu\text{m}$ . Due to the poor hole mobility, lateral hole spreading is very small and the carrier profile within the quantum wells is also confined to the injection aperture. Figure 3 illustrates this situation for the device with 2  $\mu\text{m}$  ITO aperture. Due to the narrowly confined carrier density, positive optical gain is only provided within the quantum well for  $r < 1.5 \mu\text{m}$ . Beyond that radius, the optical mode experiences strong quantum well absorption leading to a net modal gain below zero. Thus, the 2- $\mu\text{m}$  VCSEL never reaches threshold in our simulation. In the following, we therefore focus our investigation on the VCSELs with 10  $\mu\text{m}$  injection aperture which have much better chances to lase.

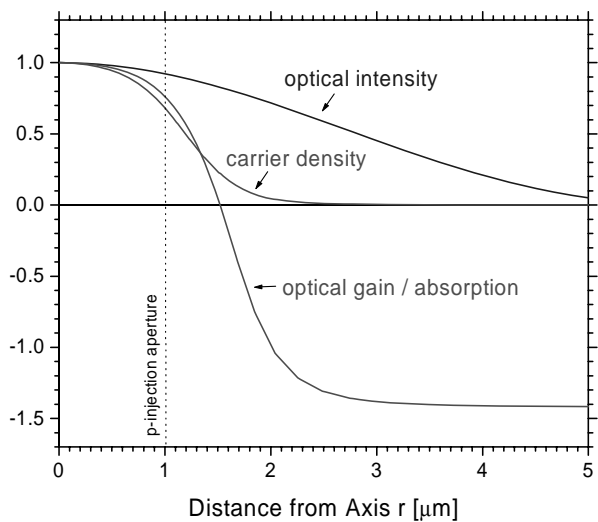


Fig. 3: Normalized lateral profiles within the quantum well for 2  $\mu\text{m}$  current injection aperture.

### 4.2 Polarization Effects

Figure 4 compares the MQW energy band diagrams as calculated with and without the built-in polarization charges given in Table 2. Without polarization, the quantum wells are almost rectangular and the AlGaN layer imposes a considerable energy barrier of 250 meV on electrons leaking out of the MQW active region. With full polarization, the energy band diagram is significantly deformed. This deformation is even more remarkable considering the high injection current density of  $j = 50 \text{ kA/cm}^2$  used here, which is 16 times higher than the threshold current density of similar edge-emitting lasers.<sup>5</sup> Surprisingly, even with strong carrier injection, the built-in polarization field is not completely screened as commonly assumed for laser operation.

To further evaluate this finding, we plot the corresponding electrostatic field profile in Fig. 5 and the free carrier densities in Fig. 6. The polarization charge densities at the MQW interfaces translate into a built-in quantum well field of 1.8 MV/cm. The actual electrostatic field within the quantum wells is about 0.5 MV/cm due to partial screening. As expected, electrons and holes are clearly separated within the quantum wells. However, even with a current density of 50  $\text{kA/cm}^2$ , the injected quantum well carrier density is not large enough to completely screen the built-in field. This can be easily checked by converting the interface charge densities given in Tab. 2 into a *uniform* quantum well carrier

density of  $2.4 \times 10^{19} \text{ cm}^{-3}$  needed for full screening. Our calculations show that current densities of more than  $100 \text{ kA/cm}^2$  are required for complete screening of the quantum well polarization field in our device.

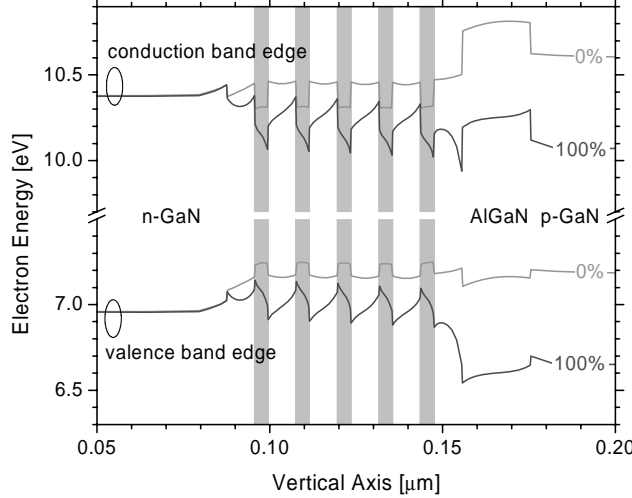


Fig. 4: MQW energy band diagram at the VCSEL axis with (100%) and without (0%) the built-in polarization charges given in Table 2 (grey: quantum wells).

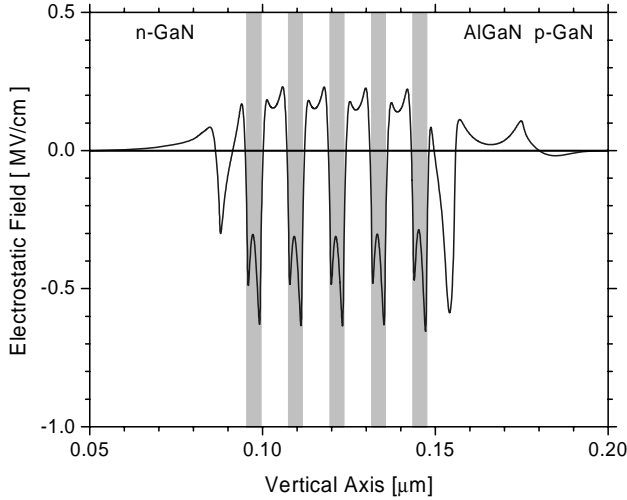


Fig. 5: Electrostatic field at the VCSEL axis with full polarization and  $50 \text{ kA/cm}^2$  current density (grey: quantum wells).

Figure 6 also illustrates the carrier accumulation at the AlGaN stopper layer. This layer is intended to prevent electrons from leaking into the p-GaN layer by creating an energy barrier in the conduction band. The energy barrier is 250 meV high without polarization (cf. Fig. 4). With full polarization, it is substantially reduced by the high density of positive polarization charges at the InGaN/AlGaN interface (cf. Tab. 2) which attract a high electron density leading to strong band bending. The corresponding increase in electron leakage is expected to have detrimental effects on the VCSEL threshold current.

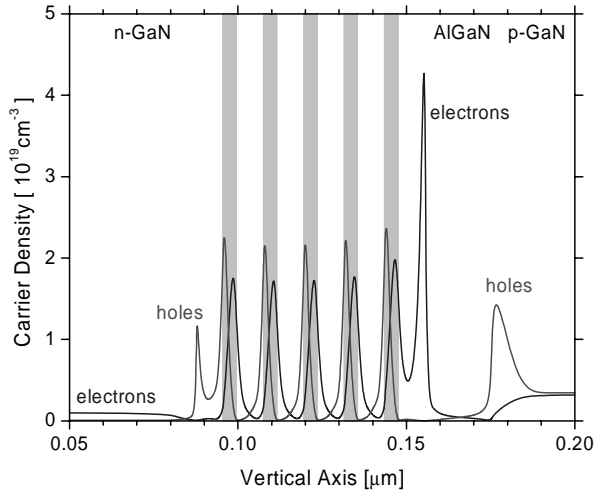


Fig. 6: Carrier density at the VCSEL axis with full polarization and  $50 \text{ kA}/\text{cm}^2$  current density (grey: quantum wells).

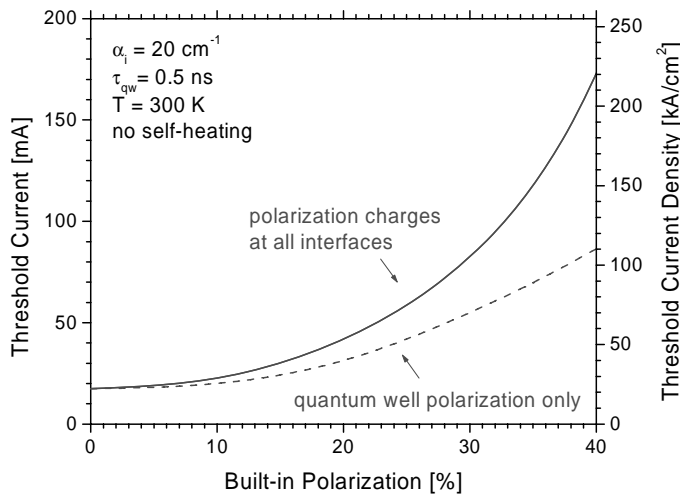


Fig. 7: VCSEL threshold as function of polarization strength (100% = Table 2).

Figure 7 shows the calculated VCSEL threshold current as function of polarization strength with 100% corresponding to the theoretically predicted values of Table 2. Without polarization, the threshold current is 17 mA. Experimentally, these VCSELs suffered from catastrophic short circuiting at about half that current, probably due to threading dislocations.<sup>2</sup> Considering only the quantum well polarization (dashed line in Fig. 7), 40% polarization enlarges the threshold current by factor 5, which is mainly due to the reduced overlap of electron and hole wave functions (cf. Fig. 6). With polarization charges at all hetero-interfaces (solid line in Fig. 7), the threshold current is increased by factor 9. The difference is mostly attributed to electron leakage across the AlGaN stopper layer. The leakage current density calculated above the stopper layer is shown in Fig. 8 for different polarization cases and  $j = 10 \text{ kA}/\text{cm}^2$ . Without polarization, the electron leakage accounts for a very small part of the total current. With 40% polarization, the electron leakage is 30 times stronger and it amounts to about half of the total current. In other words, almost half of the injected holes recombine with electrons before reaching the active region. Such leakage effects are also indicated by the measured photoluminescence spectrum of our VCSEL<sup>2</sup> as well as by investigations on similar devices.<sup>15</sup>

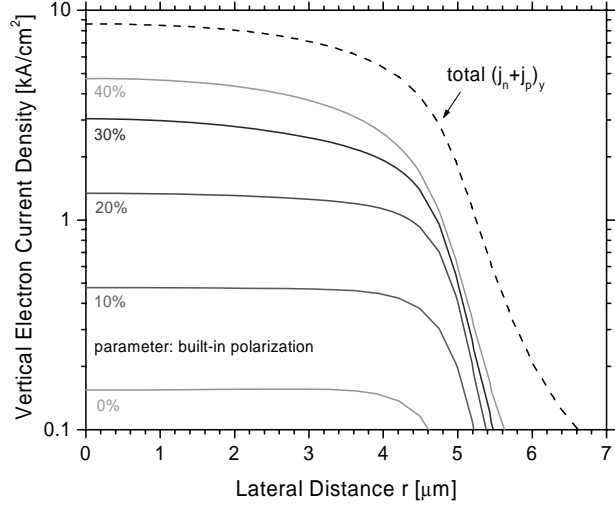


Fig. 8: Lateral profile of the vertical electron leakage current at the AlGaN/GaN interface for different polarization cases (100% = Table 2,  $j = 10 \text{ kA/cm}^2$ ).

### 4.3 Thermal Effects

Thus far, we considered pulsed laser operation assuming that the current pulses are short enough to prevent any significant self-heating of the device. Practical pulse lengths are between 50 ns and 500 ns.<sup>2</sup> We now investigate the validity of this assumption by separately solving the heat flux equation for our device. Thermal simulations need to include the entire VCSEL while optical and electrical simulations can be restricted to the active device center. We here employ the multi-physics finite-element solver FEMLAB.<sup>6</sup> The thermal conductivity of GaN is well investigated but data for the other materials in our device are hard to obtain. The values given in Table 1 are therefore approximations, accounting for the strong phonon scattering within amorphous, polycrystalline, and alloyed materials as well as at hetero-interfaces. The total heat power is estimated as product of injected current (10 mA) and measured device bias (20V) and it is assumed to be generated within the 10  $\mu\text{m}$  wide region between ITO contact and MQW. The device is mounted top-down onto the heat sink and the only way out for the heat goes through the two metal ring contacts used for current injection.<sup>2</sup> The resulting steady-state temperature distribution is shown in Fig. 9 showing a maximum temperature rise of 110 K in the center of the device. This number results in the thermal resistance of 550 K/W which is about one order of magnitude higher than in GaN-based inplane lasers,<sup>5</sup> but still lower than in GaAs-based VCSELs.<sup>7</sup>

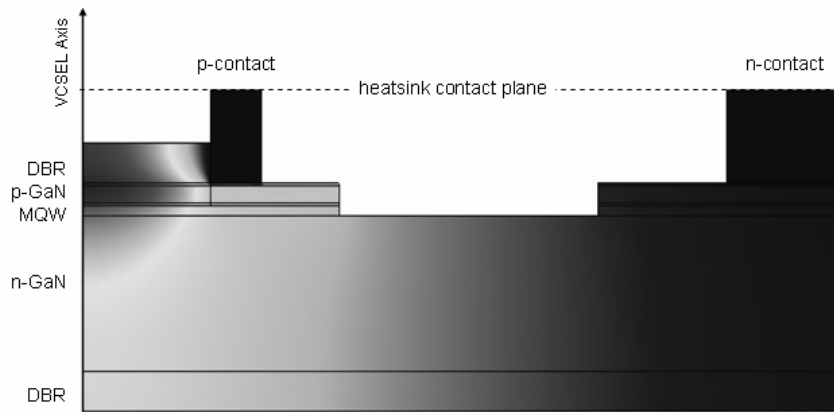


Fig. 9: Continuous-wave temperature distribution calculated for 0.2 W heat power (maximum = 410 K with heat sink at 300 K).

The transient temperature rise during pulsed laser operation is often considered negligible. Surprisingly, Fig. 10 shows that even a very short pulse of 50 ns causes a temperature rise of 26 K in the center of the device. More than half of the steady-state temperature rise is reached after only 500 ns. This temperature rise causes a reduction of the quantum well gain which further increases the threshold current.

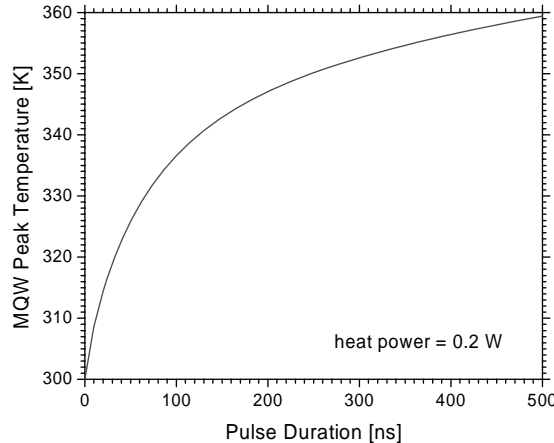


Fig. 10: Rise of the peak VCSEL temperature as function of pulse length.

## 5. SUMMARY

We have investigated internal physical mechanisms that prevent current-injected GaN-based VCSELs from lasing. The VCSELs with small injection aperture mainly suffer from poor current spreading due to the low hole mobility. In VCSELs with larger aperture, built-in polarization and subsequent gain reduction and electron leakage are the main obstacles to lasing. Even short current pulses cause considerable heating within the device.

## ACKNOWLEDGEMENT

This work was partially funded by the US Department of Energy and by the Solid State Lighting and Display Center at UCSB.

## REFERENCES

- 
- <sup>1</sup> A. V. Nurmikko and J. Han, "Progress in Blue and Near-Ultraviolet Vertical-Cavity Emitters: A Status Report," in: *Vertical-Cavity Surface-Emitting Laser Devices*, eds. H. Li and K. Iga, Springer, Berlin, 2003.
- <sup>2</sup> Tal Margalith, "Development of Growth and Fabrication Technology for Gallium Nitride-Based Vertical-Cavity Surface-Emitting Lasers," Ph.D. Dissertation, Materials Department, University of California, Santa Barbara, 2002.
- <sup>3</sup> J. Piprek, Y.A.Akulova, D.I.Babic, L.A.Coldren, and J.E.Bowers, "Minimum Temperature Sensitivity of 1.55-micron Vertical-Cavity Lasers at -30nm Gain Offset," *Applied Physics Letters*, vol. 72, no. 15, pp. 1814-1816 (1998).
- <sup>4</sup> PICS3D 2005.03, by Crosslight Software, Canada (<http://www.crosslight.com>).
- <sup>5</sup> J. Piprek and S. Nakamura, "Physics of high-power InGaN/GaN lasers," *IEE Proc.-Optoelectron.*, vol. 149, p. 145, 2002.

- 
- <sup>6</sup> FEMLAB 3.0 by Comsol, Sweden (<http://www.comsol.com>).
- <sup>7</sup> J. Piprek, *Semiconductor Optoelectronic Devices: Introduction to Physics and Simulation*, Academic Press, San Diego, 2003.
- <sup>8</sup> J. Piprek, "Simulation of GaN-based Light Emitting Devices," in: *Simulation of Semiconductor Processes and Devices* (ed. G. Wachutka and G. Schrag), Springer Verlag, Wien, 2004.
- <sup>9</sup> V. Fiorentini, F. Bernardini, and O. Ambacher, "Evidence for nonlinear macroscopic polarization in III-V nitride alloy heterostructures," *Appl. Phys. Lett.*, vol. 80, pp. 1204-1206, 2002.
- <sup>10</sup> S. F. Chichibu, A. C. Abare, M. S. Minsky, S. Keller, S. B. Fleischer, J. E. Bowers, E. Hu, U. K. Mishra, L. A. Coldren, and S. P. DenBaars, and T. Sota, "Effective band gap inhomogeneity and piezoelectric field in InGaN/GaN multiquantum well structures," *Appl. Phys. Lett.*, vol. 73, pp. 2006-2008, 1998.
- <sup>11</sup> F. Renner, P. Kiesel, G. H. Döhler, M. Kneissl, C. G. Van de Walle, and N. M. Johnson, "Quantitative analysis of the polarization fields and absorption changes in InGaN/GaN quantum wells with electroabsorption spectroscopy," *Appl. Phys. Lett.*, vol. 81, pp. 490-492, 2002.
- <sup>12</sup> H. Zhang, E. J. Miller, E. T. Yu, C. Poblenz and J. S. Speck, "Measurement of polarization charge and conduction-band offset at InGaN/GaN heterojunction interfaces," *Appl. Phys. Lett.*, vol. 84, pp. 4644-4646, 2004.
- <sup>13</sup> J. P. Ibbetson,a) P. T. Fini, K. D. Ness, S. P. DenBaars, J. S. Speck, and U. K. Mishra, "Polarization effects, surface states, and the source of electrons in AlGaN/GaN heterostructure field effect transistors, *Appl. Phys. Lett.*, vol. 77, 250 (2000).
- <sup>14</sup> I. H. Brown, I. A. Pope, P. M. Smowton, P. Blood, J. D. Thomson, W. W. Chow, D. P. Bour, and M. Kneissl, "Determination of the piezoelectric field in InGaN quantum wells," *Appl. Phys. Lett.*, vol. 86, 131108, 2005.
- <sup>15</sup> J. Piprek and S. Li, "GaN-based Light Emitting Diodes," Chapter 10 in: *Optoelectronic Devices: Advanced Simulation and Analysis*, J. Piprek (ed.), Springer Verlag, New York, 2005.